

Electronic Supplementary Information

A first-principles understanding of the CO-assisted NO reduction on the IrRu/Al₂O₃ catalyst in O₂-rich condition

Malik Waqar Arshad^{1,2}, Dong Hun Kim³, Young-Woo You^{3,4}, Soo Min Kim^{2,3,4}, Il Jeong Heo^{3,4*}
Seok Ki Kim^{1,2*}

¹C1 Gas & Carbon Convergent Research Center, Korea Research institute of Chemical Technology (KRICT), 141 Gajeong-ro, Yuseong-gu, Daejeon 34114, Republic of Korea.

²University of Science & Technology, Advanced Materials and Chemical Engineering Technology (UST), 217 Gajeong-ro, Yuseong-gu, Daejeon 34113, Republic of Korea.

³Environment & Sustainable Resources Research Center, Korea Research institute of Chemical Technology (KRICT), 141 Gajeong-ro, Yuseong-gu, Daejeon 34114, Republic of Korea.

⁴Convergent Chemistry of Air Pollution Center, Korea Research institute of Chemical Technology (KRICT), 141 Gajeong-ro, Yuseong-gu, Daejeon 34114, Republic of Korea.

*Corresponding authors: skkim726@kRICT.re.kr, zaiseok@kRICT.re.kr

List of Figures

Fig. S1. Optimized geometry (a) Ir (111) primitive cell with bader charges (b) Ir₆₄ (111) supercell (c) Ru (001) primitive cell with bader charges and (d) Ru₆₄ (001) supercell. Green and orange balls represent the Ir and Ru, respectively. 5

Fig. S2. Optimized bulk alloy models used for lattice parameter analysis (a) Ir₃Ru₁ primitive cell with bader charges (b) Ir₄₈Ru₁₆ supercell (c) Ru₃Ir₁ primitive cell with bader charges (d) Ru₄₈Ir₁₆ supercell. Green and orange balls represent the Ir and Ru, respectively. 5

Fig. S3. Optimized bulk alloy slab models used for surface oxygen analysis. O* was adsorbed on three fold hollow hcp site.(a) Ir₆₄O₁(111) super cell (b) Ru₆₄O₁ (001) supercell (c) Ir₄₈Ru₁₆O₁(111) super cell (d) Ru₄₈Ir₁₆O₁ supercell. Green, orange, and red balls represent the Ir, Ru, and oxygen, respectively. 6

Fig. S4. Optimized surface oxygen Ir-slab model with different adsorbates at their stable sites. O* was adsorbed on hcp hollow site and most stable site of each adsorbate is mention under each figure. Green, red, brown, and violet balls represent the Ir, O, C, and N, respectively. 7

Fig. S5. Optimized surface oxygen Ru-slab model with different adsorbates at their stable sites. O* was adsorbed on hcp hollow site and most stable site of each adsorbate is mention under each figure. Orange, red, brown, and violet balls represent the Ru, O, C, and N, respectively. 8

Fig. S6. Optimized surface oxygen Ir₃Ru₁-slab model with different adsorbates at their stable sites. O* was adsorbed on hcp hollow site and most stable site of each adsorbate is mention under each figure. Green, orange, red, brown, and violet balls represent the Ir, Ru, O, C, and N, respectively. 9

Fig. S7. Optimized surface oxygen Ru₃Ir₁-slab model with different adsorbates at their stable sites. O* was adsorbed on hcp hollow site and most stable site of each adsorbate is mention under each figure. Green, orange, red, brown, and violet balls represent the Ir, Ru, O, C, and N, respectively. 10

Fig. S8. Optimized surface oxygen slab models used for dominant effect study (a) Ir-Ru_{ligand} (b) Ru-Ir_{ligand} (c) Ir compressive strain (d) Ru tensile strain (e) Ir-Ru_{ensemble} (f) Ru-Ir_{ensemble} models. Green, orange, and red balls represent the Ir, Ru, and O, respectively. 11

Fig. S9. Reaction energy profile, NO+CO reactions. $T = 150\text{ }^{\circ}\text{C}$ and $P = 0.1\text{ MPa}$ 12

Fig. S10. Reaction energy profile, NO+CO+O₂ reactions. $T = 150\text{ }^{\circ}\text{C}$ and $P = 0.1\text{ MPa}$ 12

Fig. S12. Reaction energy profile of ligand effect with surface oxygen. $T = 150\text{ }^{\circ}\text{C}$ and $P = 0.1\text{ MPa}$ 13

Fig. S13. Reaction energy profile of ligand effect without surface oxygen. $T = 200\text{ }^{\circ}\text{C}$ and $P = 0.1\text{ MPa}$ 14

Fig. S14. Reaction energy profile of strain effect without surface oxygen. $T = 150\text{ }^{\circ}\text{C}$ and $P = 0.1\text{ MPa}$.14

Fig. S15. Reaction energy profile of strain effect with surface oxygen. $T = 150\text{ }^{\circ}\text{C}$ and $P = 0.1\text{ MPa}$ 15

Fig. S16. Reaction energy profile of strain effect without surface oxygen. $T = 200\text{ }^{\circ}\text{C}$ and $P = 0.1\text{ MPa}$ 15

Fig. S17. Reaction energy profile of dominant effect in an IrRu alloy formation without surface oxygen. $T = 150\text{ }^{\circ}\text{C}$ and $P = 0.1\text{ MPa}$ 16

Fig. S18. Reaction energy profile of dominant effect in an IrRu alloy formation with surface oxygen. $T = 150\text{ }^{\circ}\text{C}$ and $P = 0.1\text{ MPa}$ 16

Fig. S19. Reaction energy profile of dominant effect in an IrRu alloy formation without surface oxygen. $T = 200\text{ }^{\circ}\text{C}$ and $P = 0.1\text{ MPa}$	17
Fig. S20. Mean difference between the median values (E_{mid}) of the pure Ir and Ru catalysts and the energy values of the different alloy surfaces without surface oxygen. $T = 150\text{ }^{\circ}\text{C}$ and $P = 0.1\text{ MPa}$	18
Fig. S21. Mean difference between the median values (E_{mid}) of the pure Ir and Ru catalysts and the energy values of the different alloy surfaces with surface oxygen. $T = 150\text{ }^{\circ}\text{C}$ and $P = 0.1\text{ MPa}$	18
Fig. S23. Activation energy (E_a) trends for three important reactions among the different catalytic models with surface oxygen for different catalytic models. $T = 150\text{ }^{\circ}\text{C}$ and $P = 0.1\text{ MPa}$	19
Fig. S22. Activation energy (E_a) trends for three important reactions among the different catalytic models without surface oxygen for different catalytic models. $T = 150\text{ }^{\circ}\text{C}$ and $P = 0.1\text{ MPa}$	19
Fig. S24. Optimized geometry and gibbs free formation energy of CO oxidation reaction over Ir, Ru and their alloy surfaces at $T = 200\text{ }^{\circ}\text{C}$ and $P = 0.1\text{ MPa}$. To calculate the formation energy, we used H_2O , N_2 , CH_4 , and H_2 as standard electronic energies. Green, orange, red, and brown balls represent the Ir, Ru, O, and C, respectively.....	20
Fig. S25. Optimized geometry and gibbs free formation energy of N_2 formation via N–N recombination reaction over Ir, Ru and their alloy surfaces at $T = 200\text{ }^{\circ}\text{C}$ and $P = 0.1\text{ MPa}$. To calculate the formation energy, we used H_2O , N_2 , CH_4 , and H_2 as standard electronic energies. Green, orange, and violet balls represent the Ir, Ru, and N, respectively.....	21
Fig. S26. Optimized geometry and gibbs free formation energy of N_2O decomposition in N_2 formation reaction over Ir, Ru and their alloy surfaces at $T = 200\text{ }^{\circ}\text{C}$ and $P = 0.1\text{ MPa}$. To calculate the formation energy, we used H_2O , N_2 , CH_4 , and H_2 as standard electronic energies. Green, orange, red, and violet balls represent the Ir, Ru, O, and N, respectively.....	22
Fig. S27. Optimized geometry and gibbs free formation energy of N_2O formation reaction over Ir, Ru and their alloy surfaces at $T = 200\text{ }^{\circ}\text{C}$ and $P = 0.1\text{ MPa}$. To calculate the formation energy, we used H_2O , N_2 , CH_4 , and H_2 as standard electronic energies. Green, orange, red, and violet balls represent the Ir, Ru, O, and N, respectively.	23
Fig. S28. Optimized geometry and gibbs free formation energy of NCO formation reaction over Ir, Ru and their alloy surfaces at $T = 200\text{ }^{\circ}\text{C}$ and $P = 0.1\text{ MPa}$. To calculate the formation energy, we used H_2O , N_2 , CH_4 , and H_2 as standard electronic energies. Green, orange, red, brown, and violet balls represent the Ir, Ru, O, C, and N, respectively.	24
Fig. S29. Optimized geometry and gibbs free formation energy of NO decomposition reaction over Ir, Ru and their alloy surfaces at $T = 200\text{ }^{\circ}\text{C}$ and $P = 0.1\text{ MPa}$. To calculate the formation energy, we used H_2O , N_2 , CH_4 , and H_2 as standard electronic energies. Green, orange, red, and violet balls represent the Ir, Ru, O, and N, respectively.....	25
Fig. S30. Optimized geometry and gibbs free formation energy of CO decomposition reaction over Ir, Ru and their alloy surfaces at $T = 200\text{ }^{\circ}\text{C}$ and $P = 0.1\text{ MPa}$. To calculate the formation energy, we used H_2O , N_2 , CH_4 , and H_2 as standard electronic energies. Green, orange, red, and brown balls represent the Ir, Ru, O, and C, respectively.....	26
Fig. S31. Optimized geometry and gibbs free formation energy of NO_2 formation reaction over Ir, Ru and their alloy surfaces at $T = 200\text{ }^{\circ}\text{C}$ and $P = 0.1\text{ MPa}$. To calculate the formation energy, we used H_2O , N_2 ,	

CH₄, and H₂ as standard electronic energies. Green, orange, red, and violet balls represent the Ir, Ru, O, and N, respectively. 27

Fig. S32. Optimized geometry and gibbs free formation energy of N₂ formation reaction over Ir, Ru and their alloy surfaces at $T = 200$ °C and $P = 0.1$ MPa . To calculate the formation energy, we used H₂O, N₂, CH₄, and H₂ as standard electronic energies. Green, orange, red, and violet balls represent the Ir, Ru, O, and N, respectively. 28

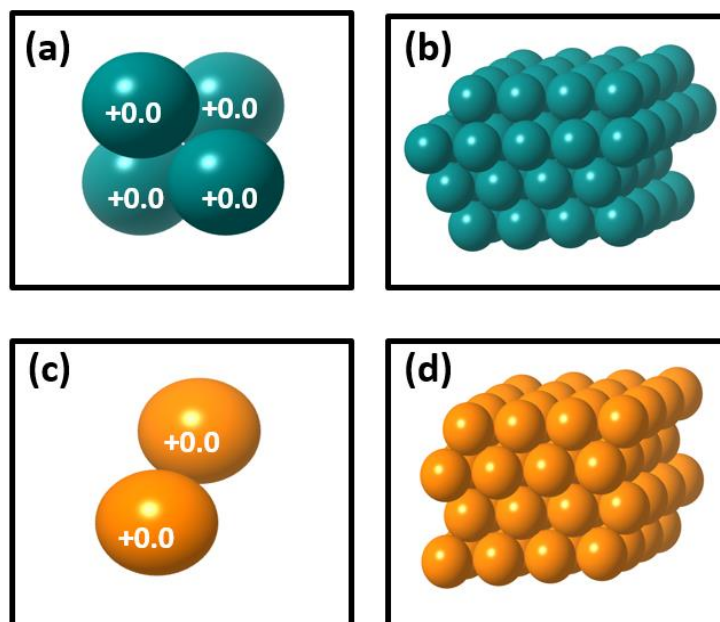


Fig. S1. Optimized geometry (a) Ir (111) primitive cell with bader charges (b) Ir₆₄ (111) supercell (c) Ru (001) primitive cell with bader charges and (d) Ru₆₄ (001) supercell. Green and orange balls represent the Ir and Ru, respectively.

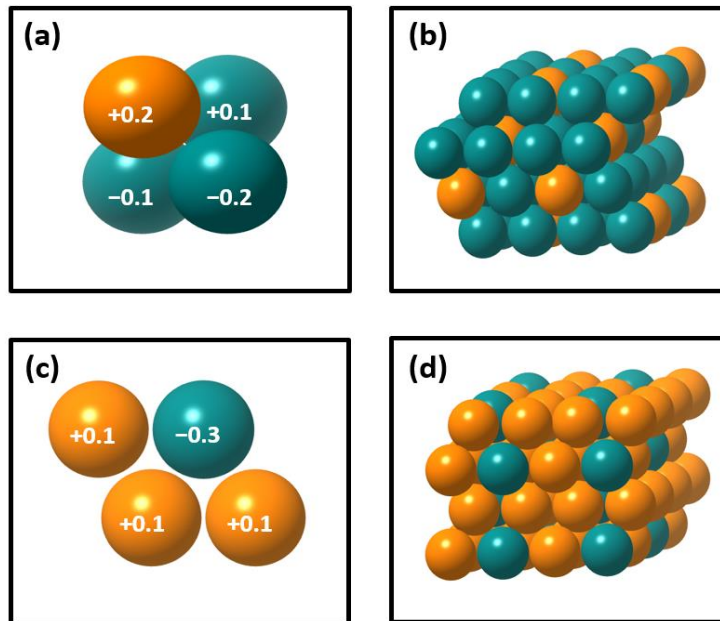


Fig. S2. Optimized bulk alloy models used for lattice parameter analysis (a) Ir₃Ru₁ primitive cell with bader charges (b) Ir₄₈Ru₁₆ supercell (c) Ru₃Ir₁ primitive cell with bader charges (d) Ru₄₈Ir₁₆ supercell. Green and orange balls represent the Ir and Ru, respectively.

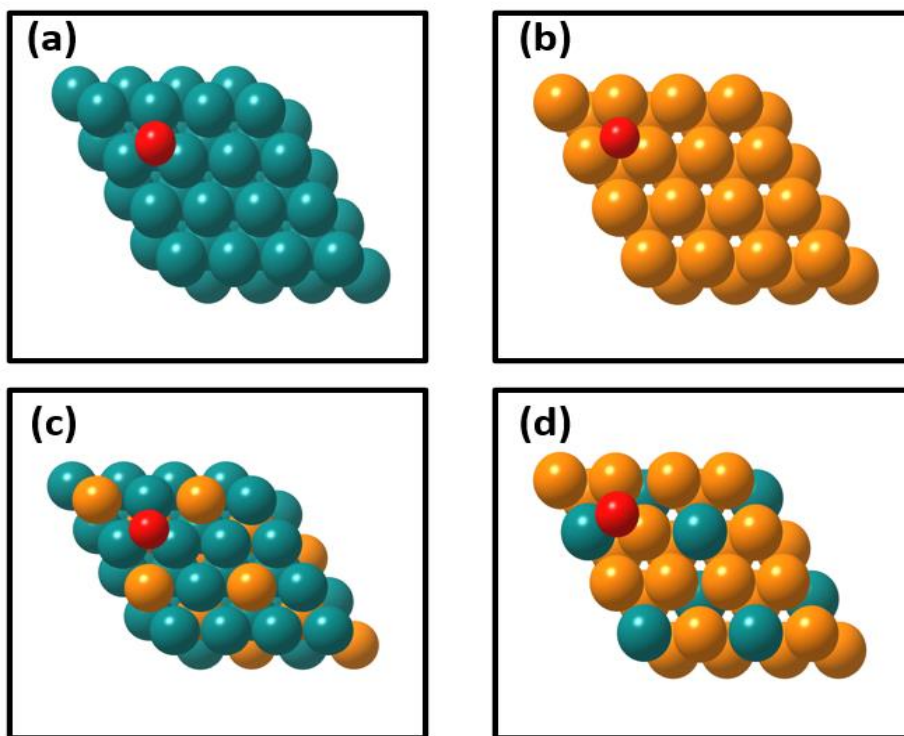


Fig. S3. Optimized bulk alloy slab models used for surface oxygen analysis. O* was adsorbed on three fold hollow hcp site.(a) $\text{Ir}_{64}\text{O}_1(111)$ super cell (b) $\text{Ru}_{64}\text{O}_1(001)$ supercell (c) $\text{Ir}_{48}\text{Ru}_{16}\text{O}_1(111)$ super cell (d) $\text{Ru}_{48}\text{Ir}_{16}\text{O}_1$ supercell. Green, orange, and red balls represent the Ir, Ru, and oxygen, respectively.

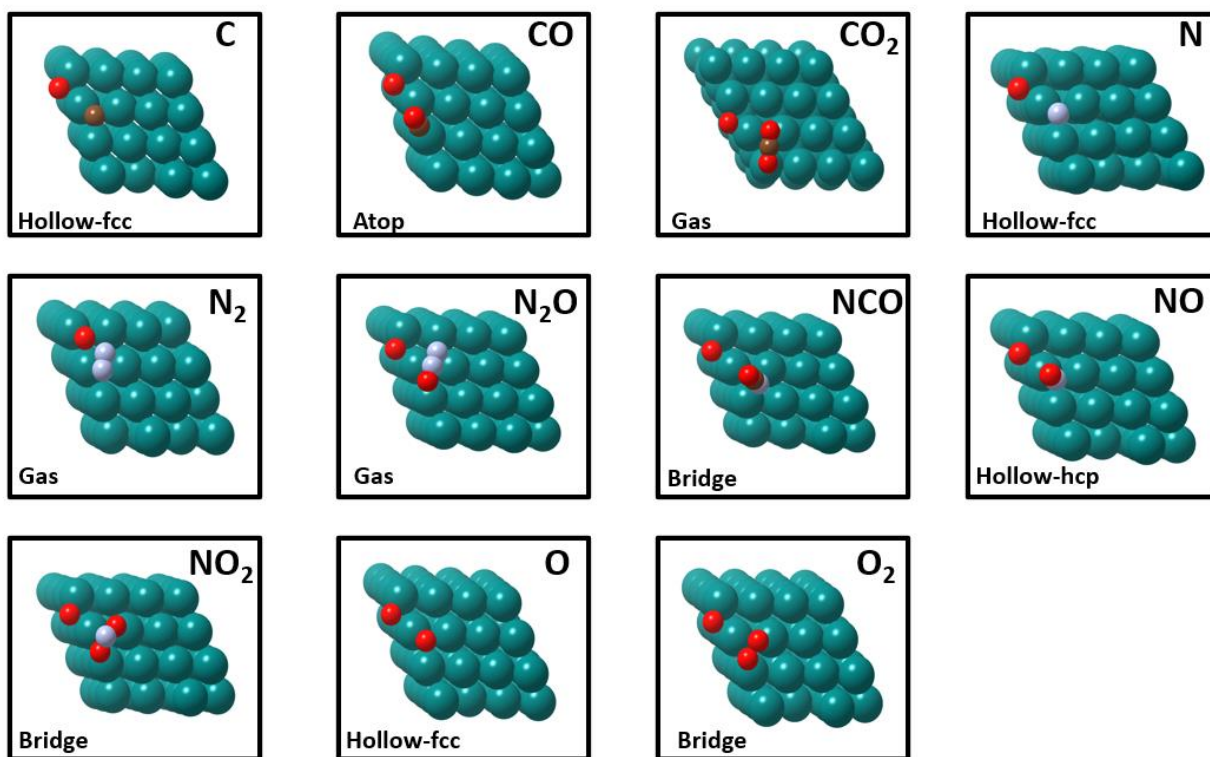


Fig. S4. Optimized surface oxygen Ir-slab model with different adsorbates at their stable sites. O* was adsorbed on hcp hollow site and most stable site of each adsorbate is mention under each figure. Green, red, brown, and violet balls represent the Ir, O, C, and N, respectively.

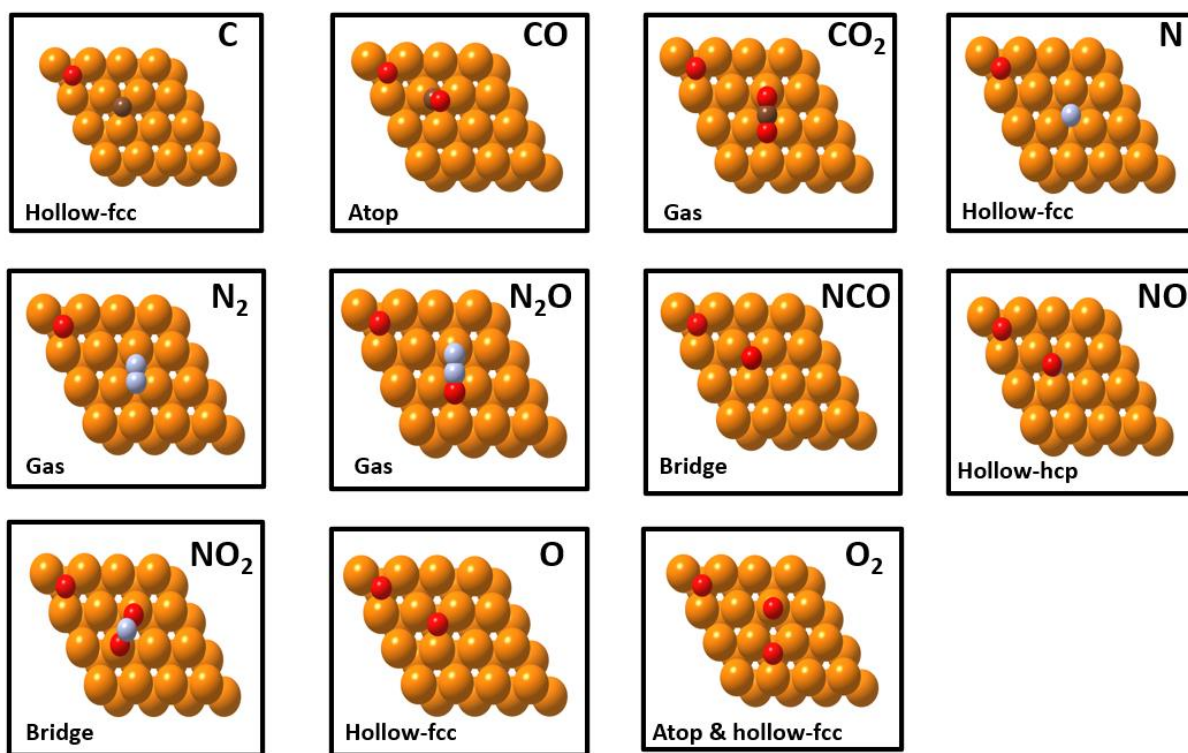


Fig. S5. Optimized surface oxygen Ru-slab model with different adsorbates at their stable sites. O* was adsorbed on hcp hollow site and most stable site of each adsorbate is mention under each figure. Orange, red, brown, and violet balls represent the Ru, O, C, and N, respectively.

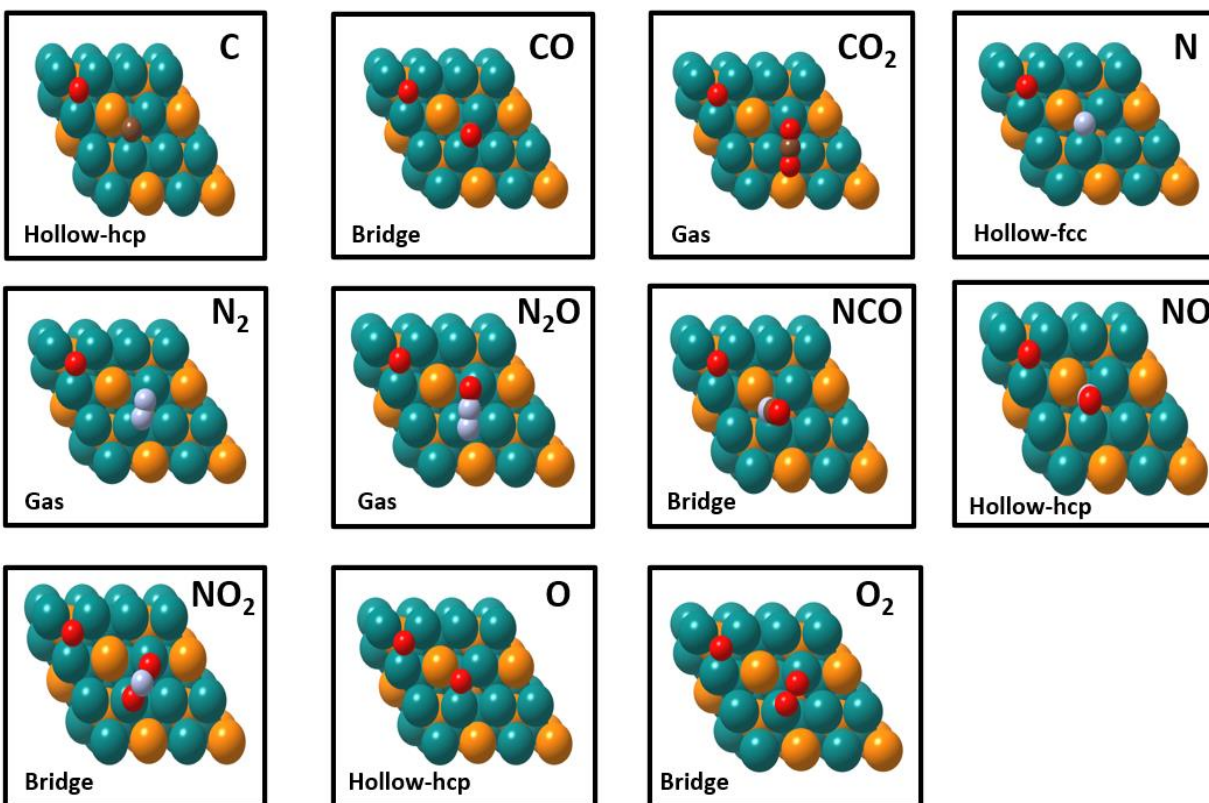


Fig. S6. Optimized surface oxygen Ir₃Ru₁-slab model with different adsorbates at their stable sites. O* was adsorbed on hcp hollow site and most stable site of each adsorbate is mention under each figure. Green, orange, red, brown, and violet balls represent the Ir, Ru, O, C, and N, respectively.

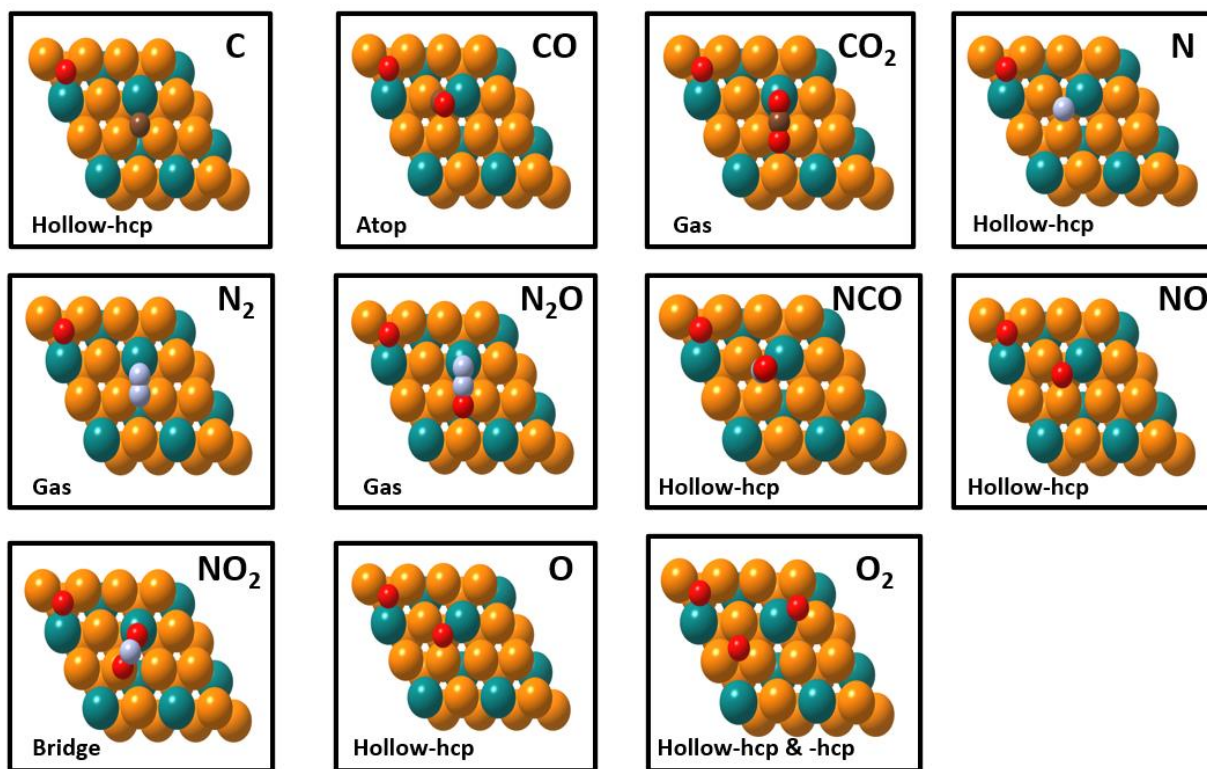


Fig. S7. Optimized surface oxygen Ru₃Ir₁-slab model with different adsorbates at their stable sites. O* was adsorbed on hcp hollow site and most stable site of each adsorbate is mention under each figure. Green, orange, red, brown, and violet balls represent the Ir, Ru, O, C, and N, respectively.

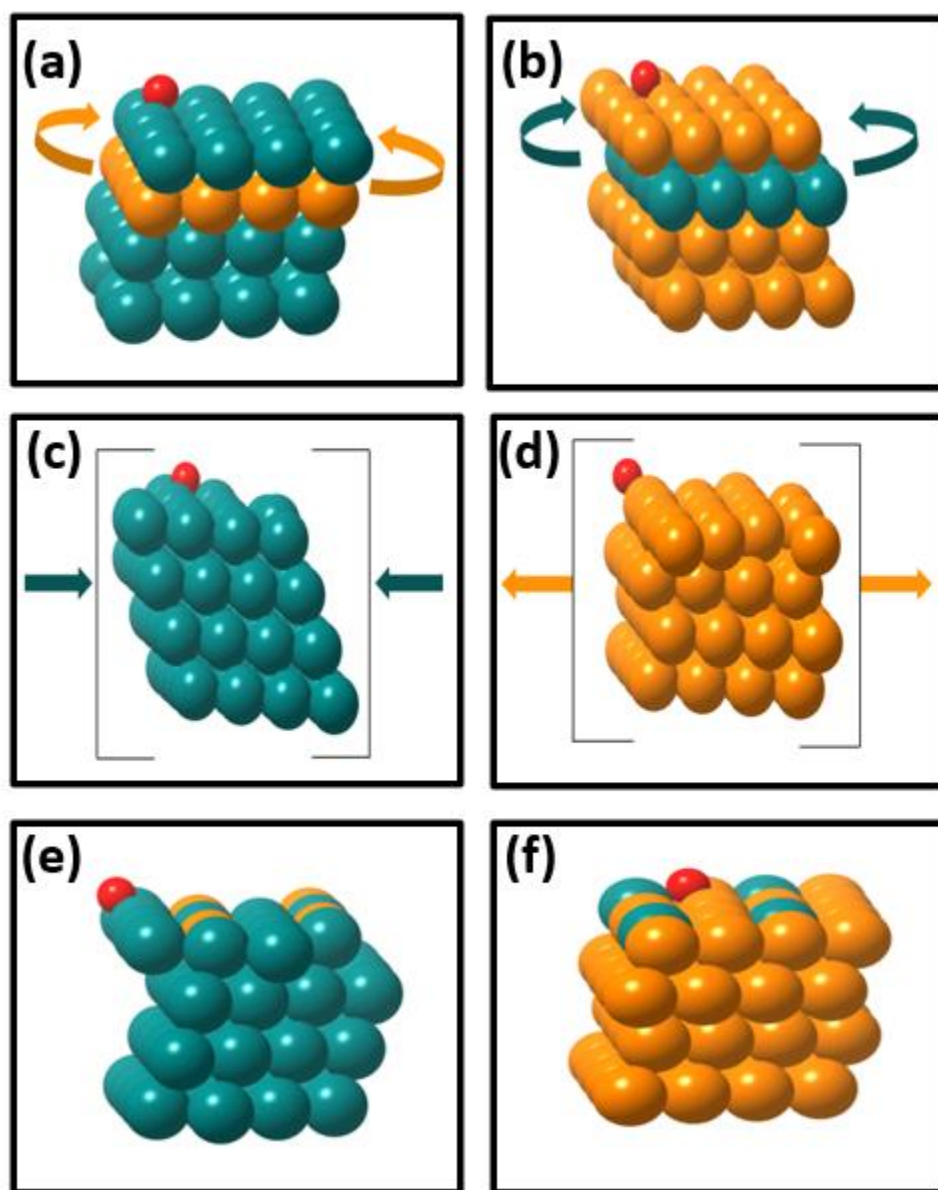


Fig. S8. Optimized surface oxygen slab models used for dominant effect study (a) Ir-Ru_{ligand} (b) Ru-Ir_{ligand} (c) Ir compressive strain (d) Ru tensile strain (e) Ir-Ru_{ensemble} (f) Ru-Ir_{ensemble} models. Green, orange, and red balls represent the Ir, Ru, and O, respectively.

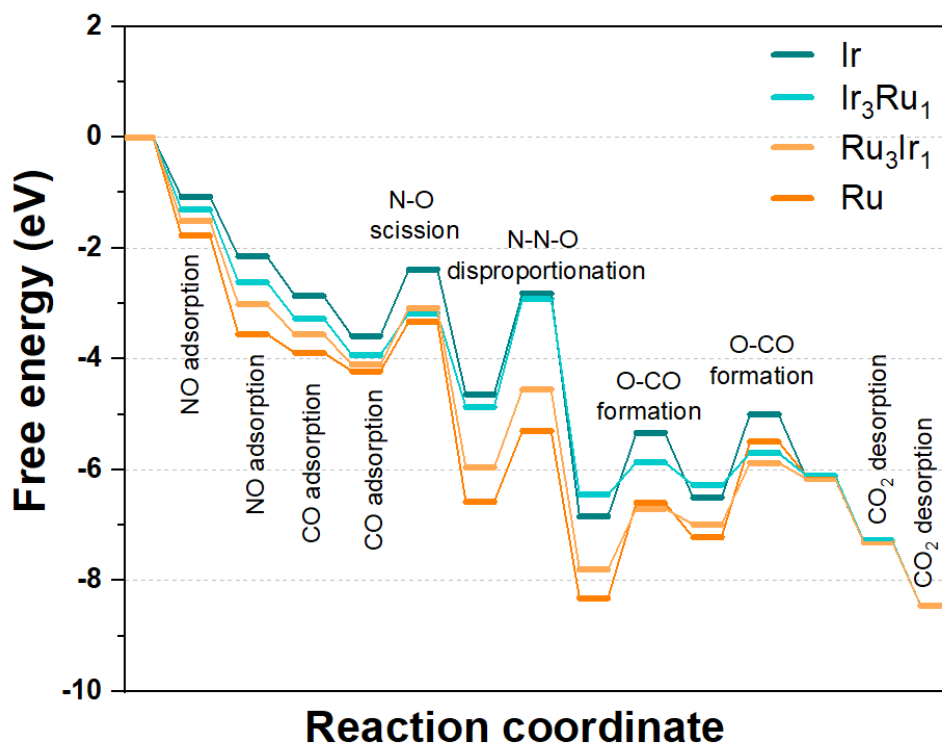


Fig. S9. Reaction energy profile, NO+CO reactions. $T = 150\text{ }^{\circ}\text{C}$ and $P = 0.1\text{ MPa}$

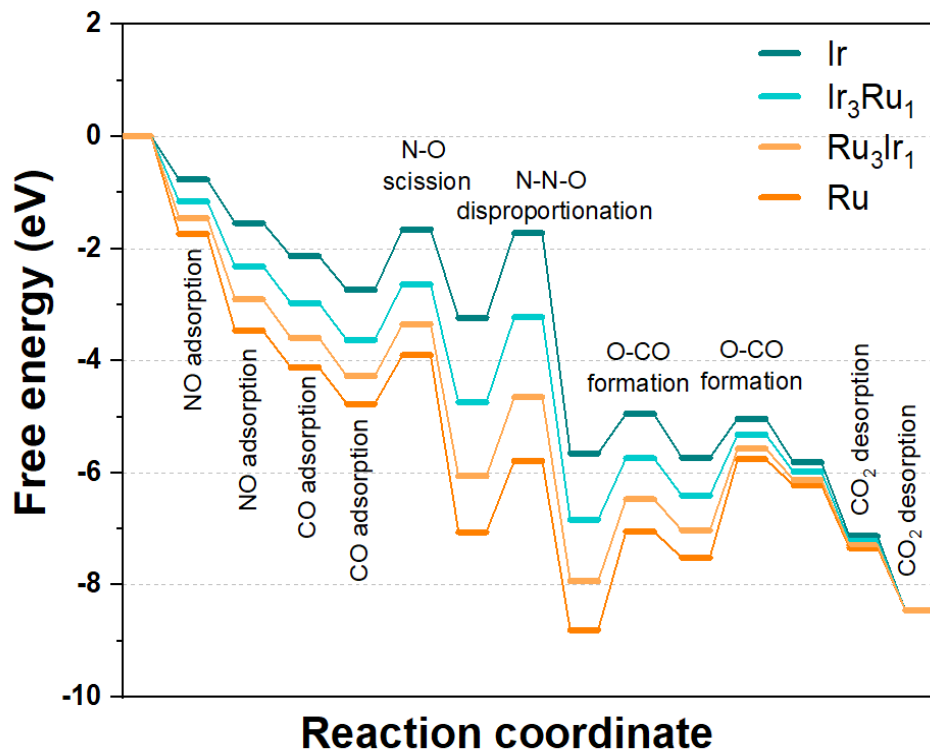


Fig. S10. Reaction energy profile, NO+CO+O₂ reactions. $T = 150\text{ }^{\circ}\text{C}$ and $P = 0.1\text{ MPa}$

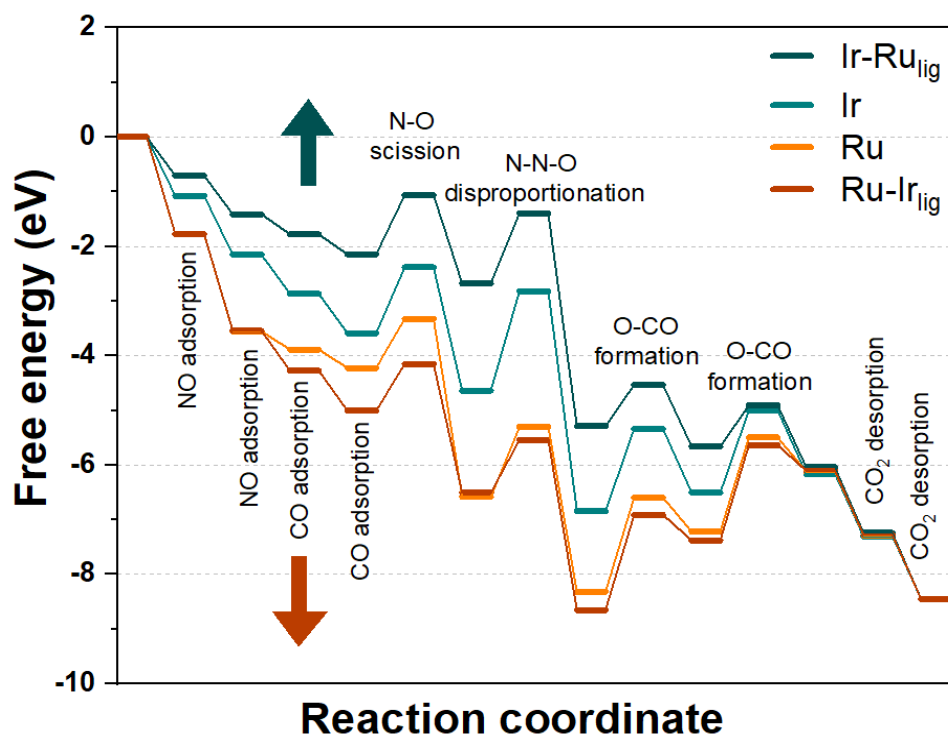


Fig. S11. Reaction energy profile of ligand effect without surface oxygen. $T = 150\text{ }^\circ\text{C}$ and $P = 0.1\text{ MPa}$

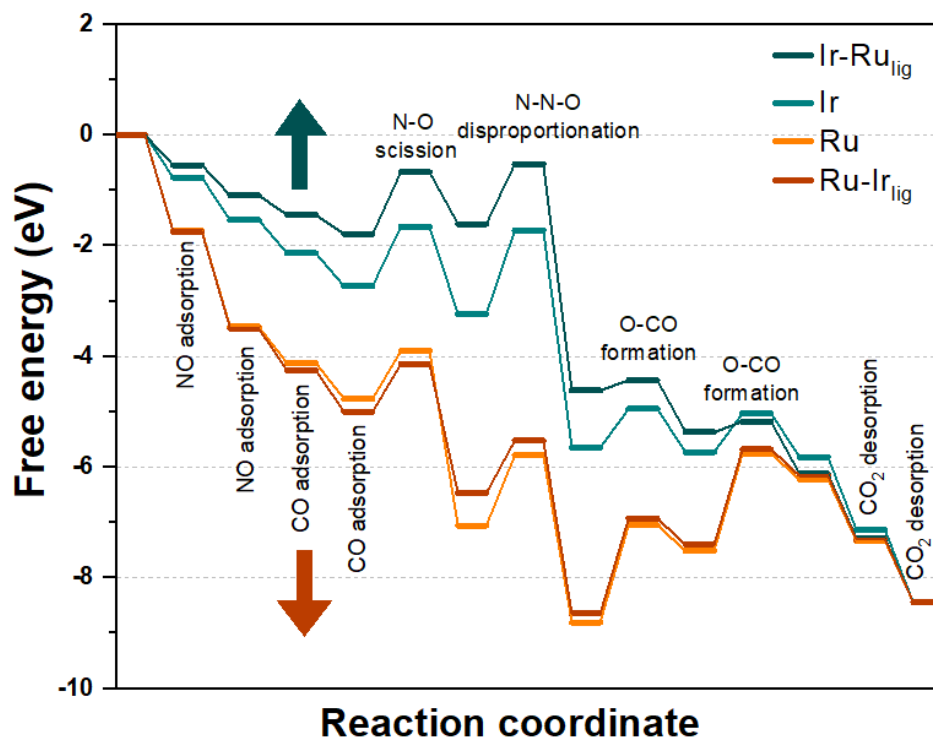


Fig. S12. Reaction energy profile of ligand effect with surface oxygen. $T = 150\text{ }^\circ\text{C}$ and $P = 0.1\text{ MPa}$

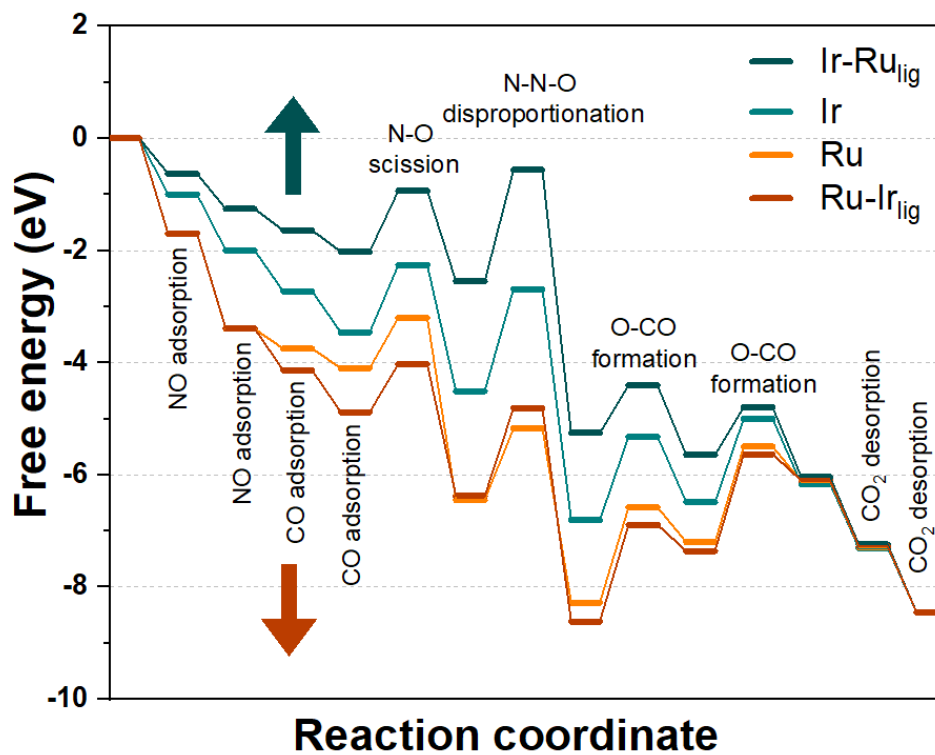


Fig. S13. Reaction energy profile of ligand effect without surface oxygen.
 $T = 200\text{ }^{\circ}\text{C}$ and $P = 0.1\text{ MPa}$

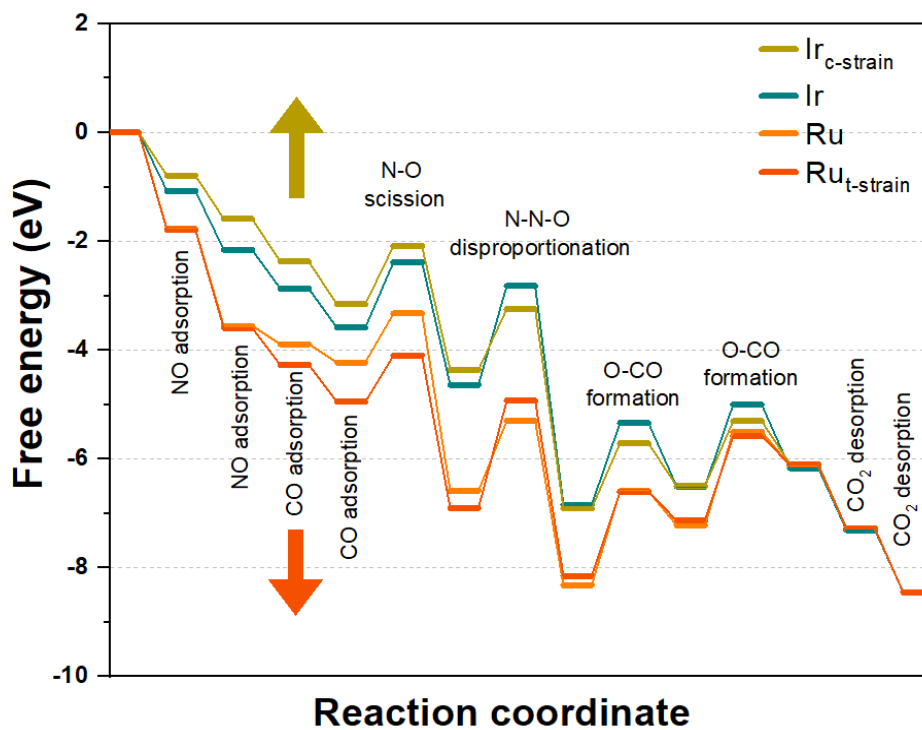


Fig. S14. Reaction energy profile of strain effect without surface oxygen.
 $T = 150\text{ }^{\circ}\text{C}$ and $P = 0.1\text{ MPa}$

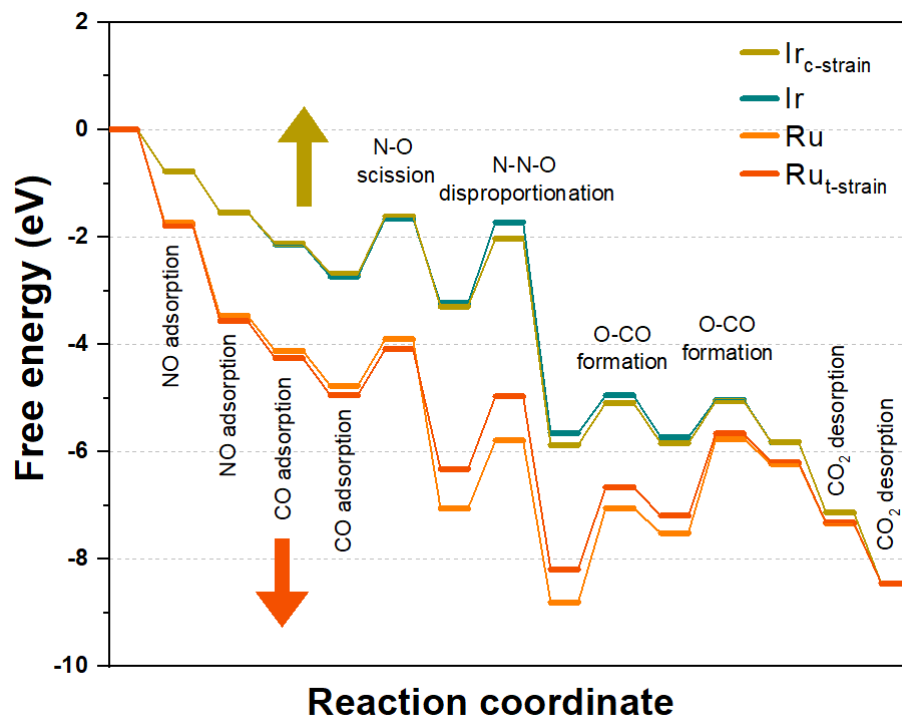


Fig. S15. Reaction energy profile of strain effect with surface oxygen.
 $T = 150\text{ }^\circ\text{C}$ and $P = 0.1\text{ MPa}$

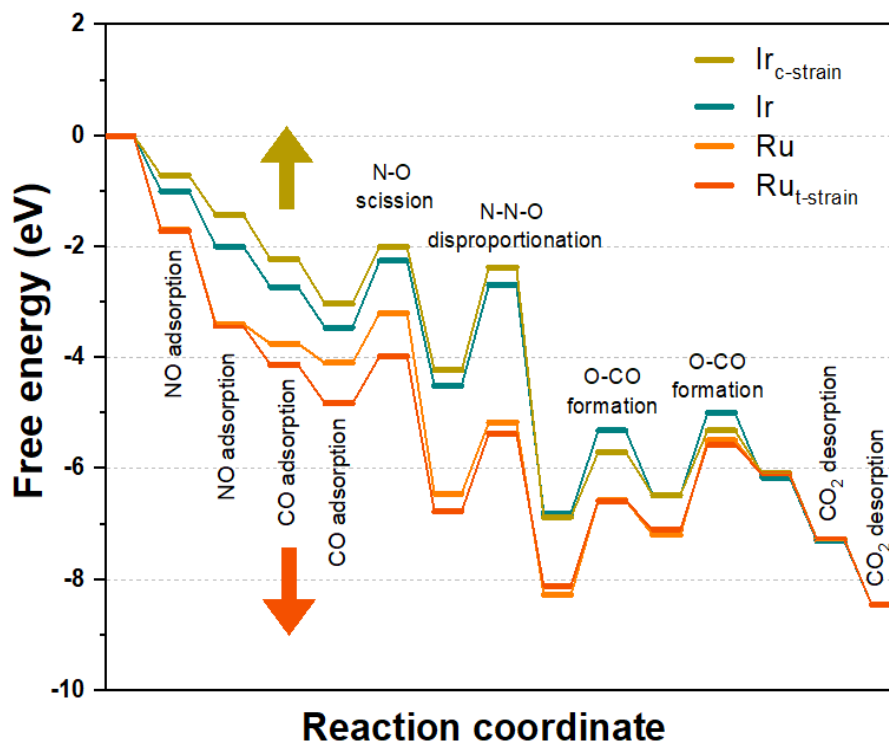


Fig. S16. Reaction energy profile of strain effect without surface oxygen.
 $T = 200\text{ }^\circ\text{C}$ and $P = 0.1\text{ MPa}$

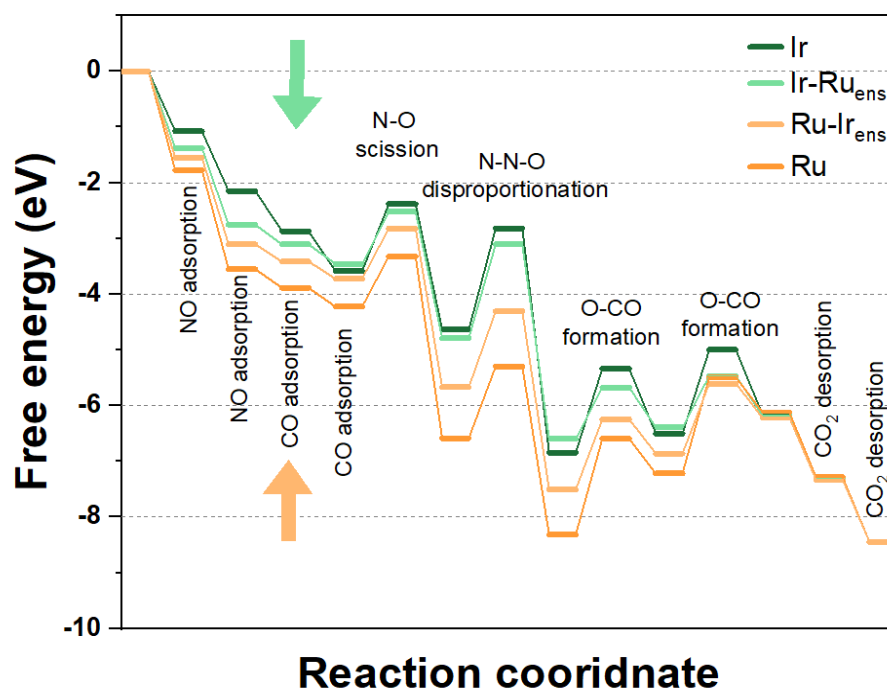


Fig. S17. Reaction energy profile of dominant effect in an IrRu alloy formation without surface oxygen. $T = 150\text{ }^{\circ}\text{C}$ and $P = 0.1\text{ MPa}$

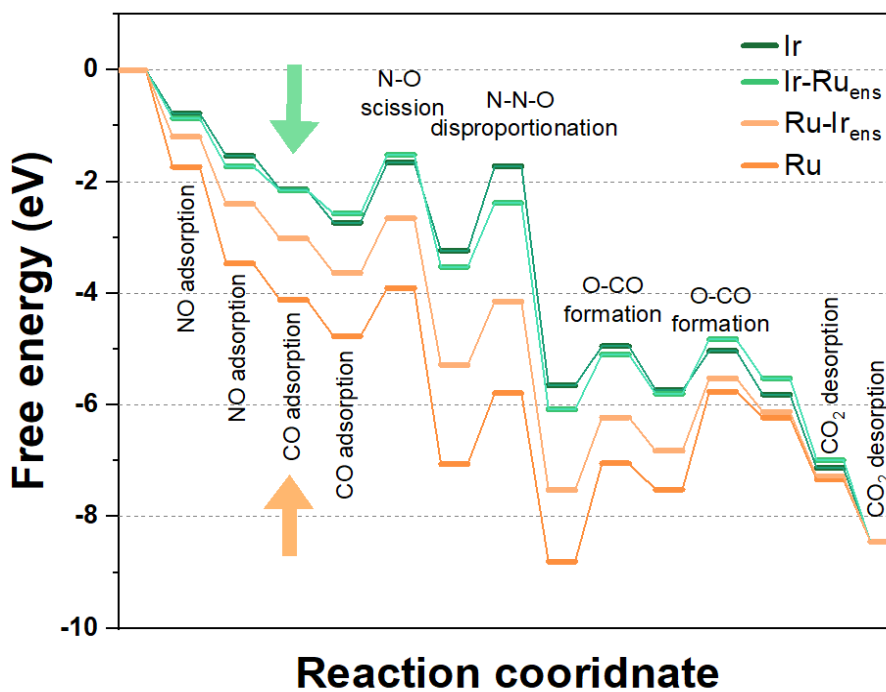


Fig. S18. Reaction energy profile of dominant effect in an IrRu alloy formation with surface oxygen. $T = 150\text{ }^{\circ}\text{C}$ and $P = 0.1\text{ MPa}$

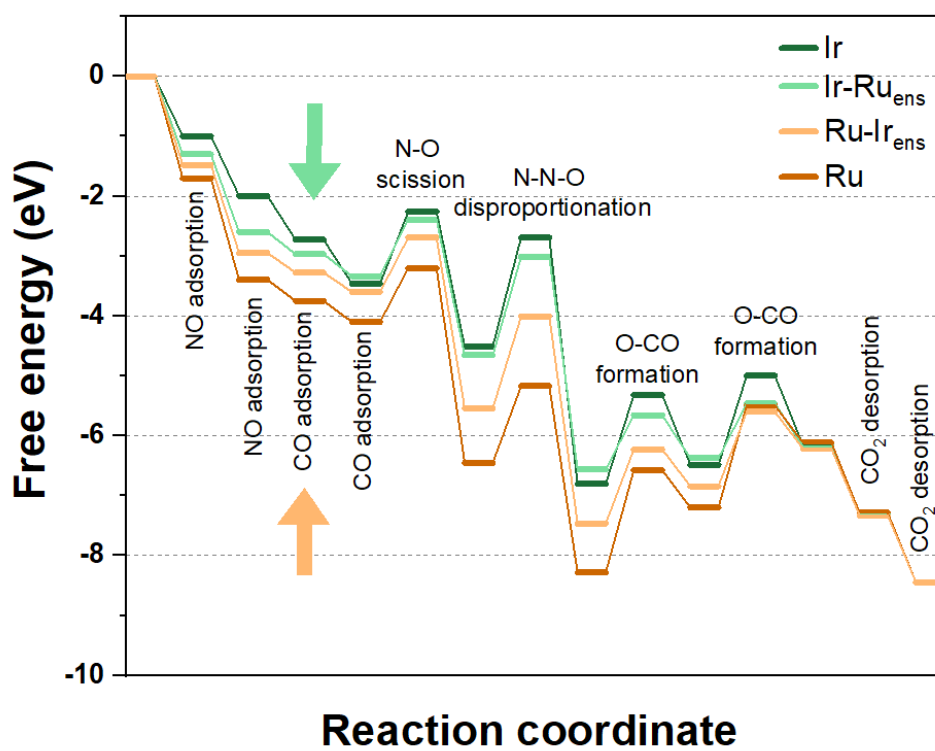
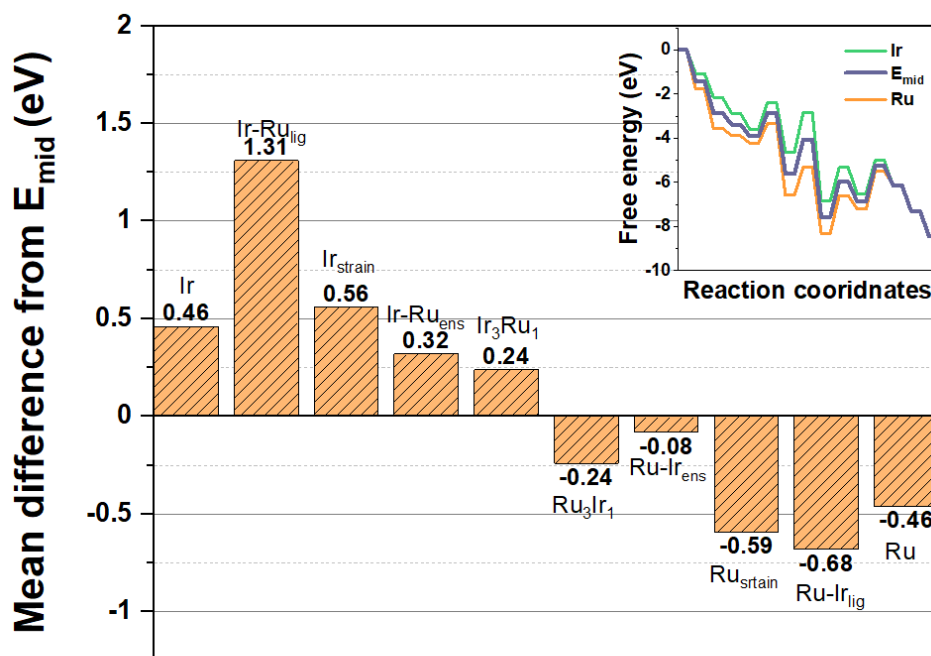
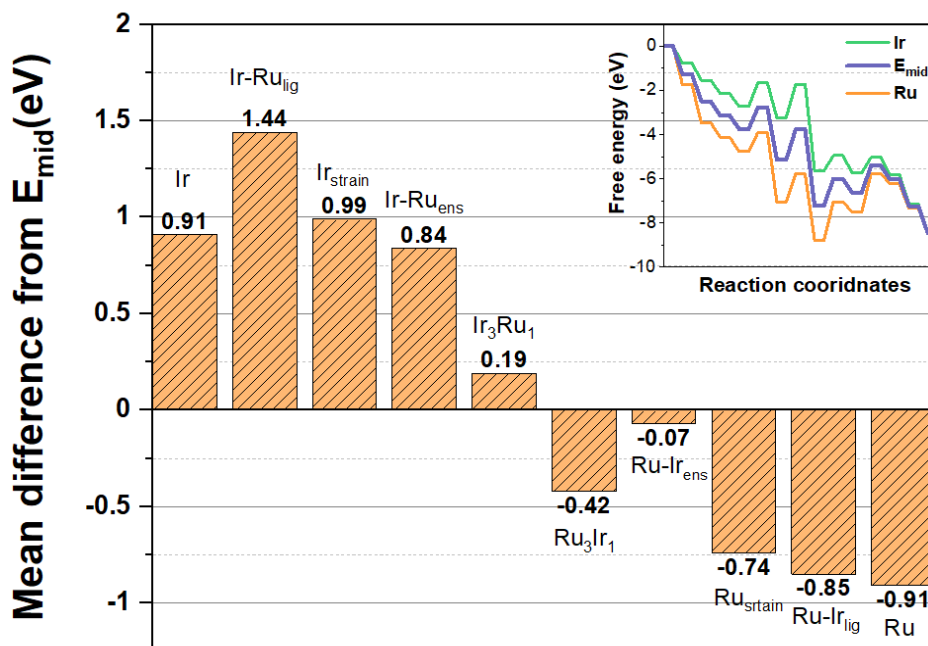


Fig. S19. Reaction energy profile of dominant effect in an IrRu alloy formation without surface oxygen. $T = 200$ °C and $P = 0.1$ MPa



Catalytic models

Fig. S20. Mean difference between the median values (E_{mid}) of the pure Ir and Ru catalysts and the energy values of the different alloy surfaces without surface oxygen. $T = 150\text{ }^{\circ}\text{C}$ and $P = 0.1\text{ MPa}$



Catalytic models

Fig. S21. Mean difference between the median values (E_{mid}) of the pure Ir and Ru catalysts and the energy values of the different alloy surfaces with surface oxygen. $T = 150\text{ }^{\circ}\text{C}$ and $P = 0.1\text{ MPa}$

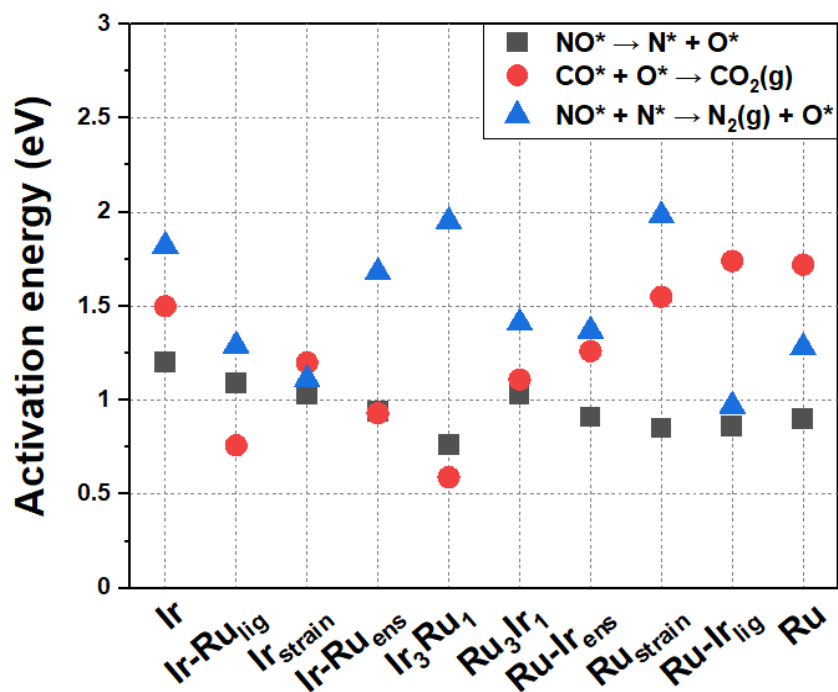


Fig. S22. Activation energy (E_a) trends for three important reactions among the different catalytic models without surface oxygen for different catalytic models. $T = 150\text{ }^\circ\text{C}$ and $P = 0.1\text{ MPa}$

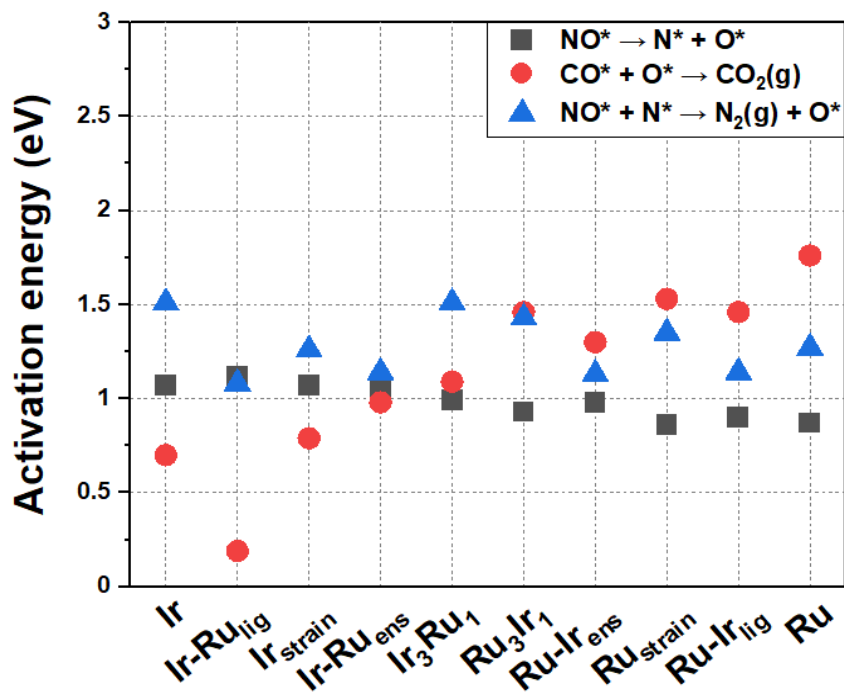


Fig. S23. Activation energy (E_a) trends for three important reactions among the different catalytic models with surface oxygen for different catalytic models. $T = 150\text{ }^\circ\text{C}$ and $P = 0.1\text{ MPa}$

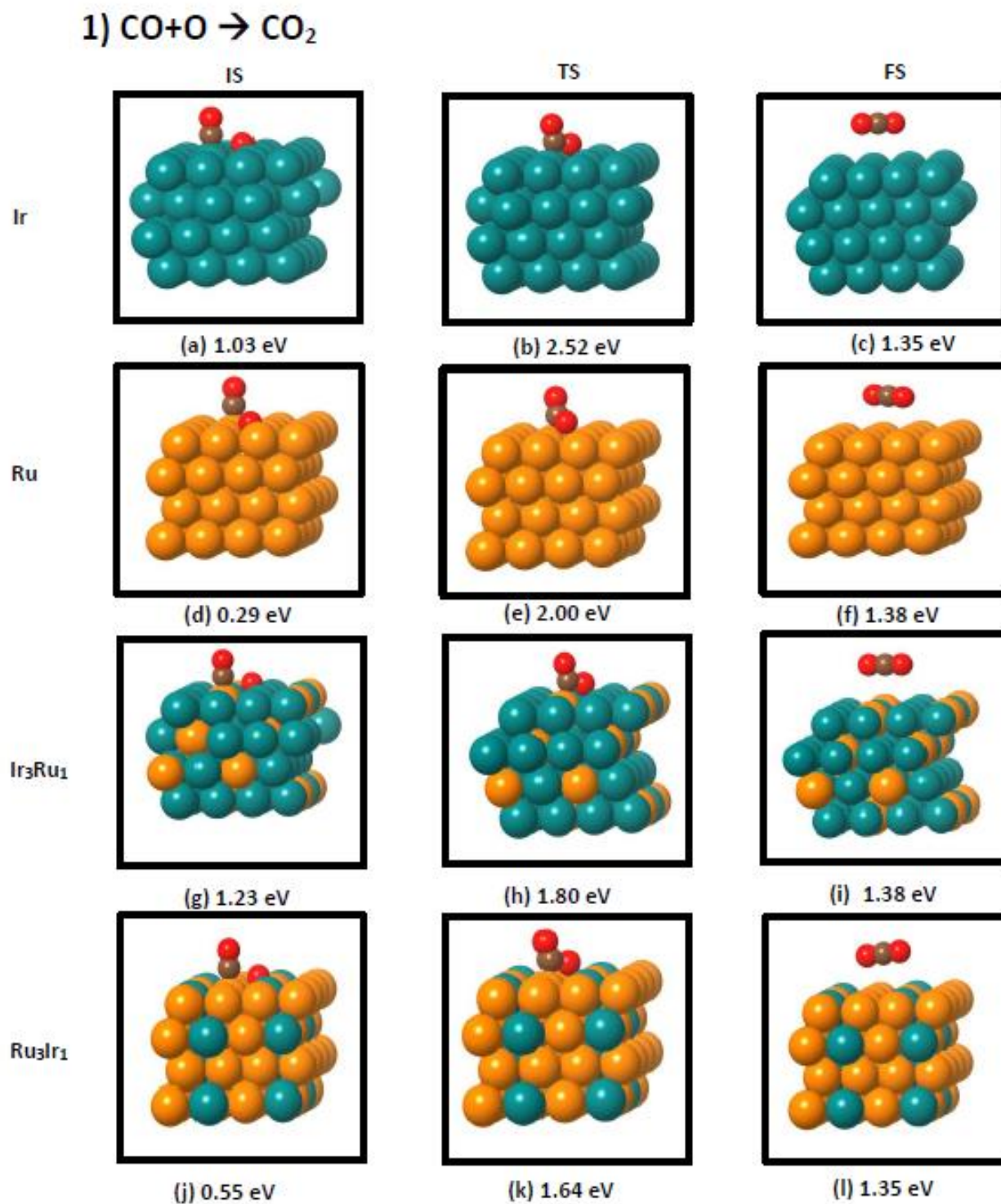


Fig. S24. Optimized geometry and gibbs free formation energy of CO oxidation reaction over Ir, Ru and their alloy surfaces at $T = 200^\circ\text{C}$ and $P = 0.1\text{ MPa}$. To calculate the formation energy, we used H_2O , N_2 , CH_4 , and H_2 as standard electronic energies. Green, orange, red, and brown balls represent the Ir, Ru, O, and C, respectively.

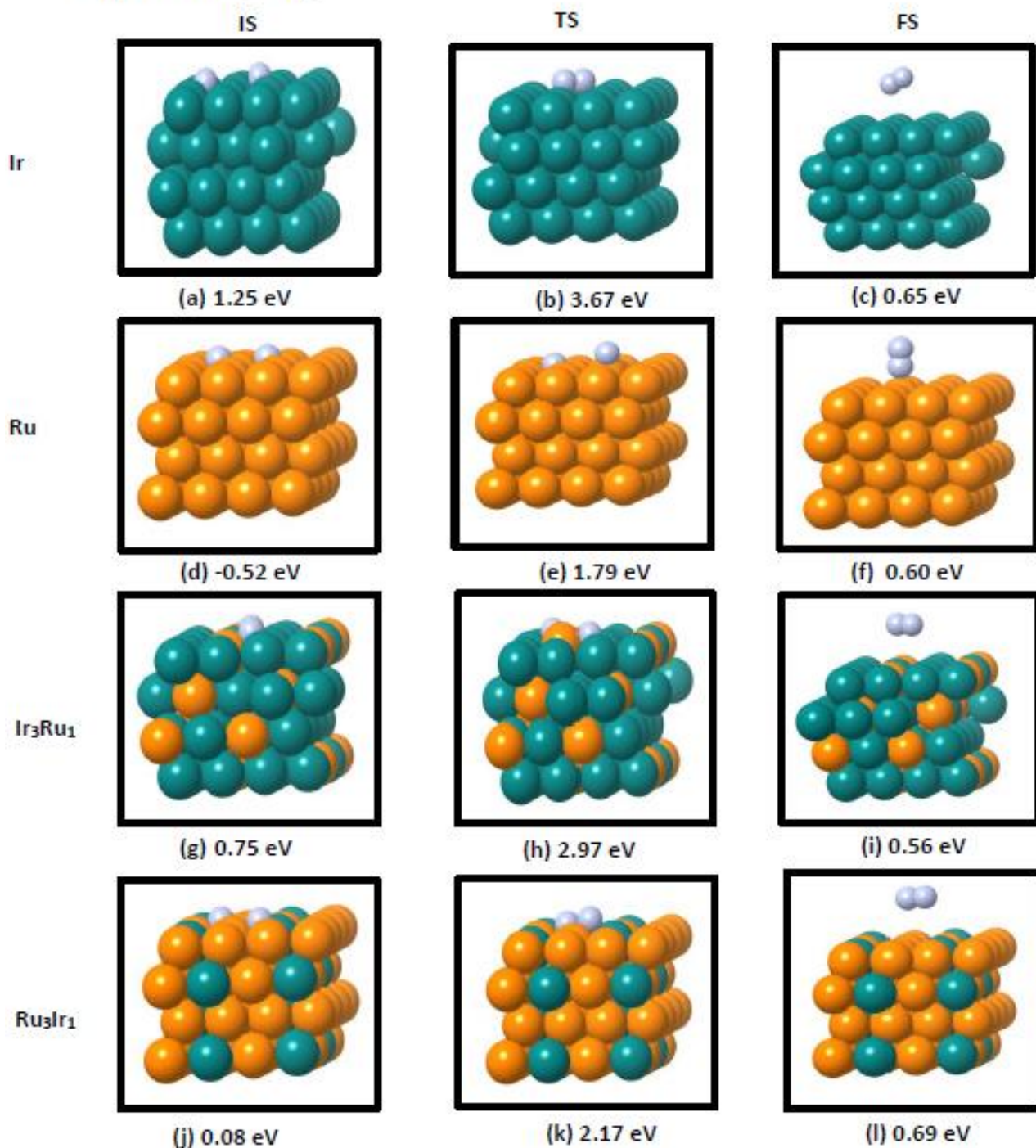


Fig. S25. Optimized geometry and gibbs free formation energy of N_2 formation via N–N recombination over Ir, Ru and their alloy surfaces at $T = 200$ °C and $P = 0.1$ MPa . To calculate the formation energy, we used H_2O , N_2 , CH_4 , and H_2 as standard electronic energies. Green, orange, and violet balls represent the Ir, Ru, and N, respectively.

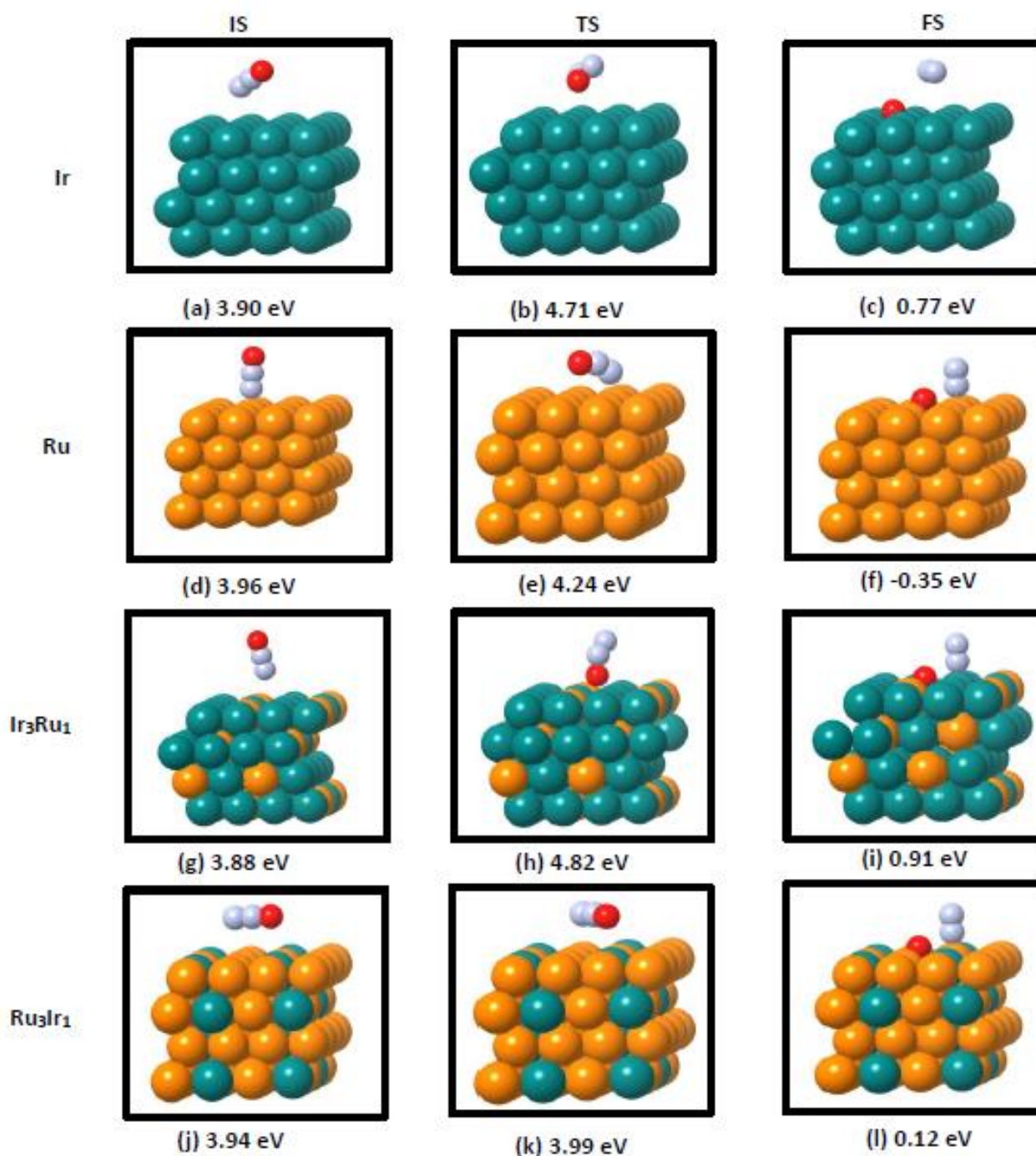
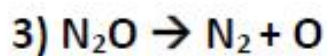


Fig. S26. Optimized geometry and gibbs free formation energy of N_2O decomposition in N_2 formation reaction over Ir, Ru and their alloy surfaces at $T = 200\text{ }^\circ\text{C}$ and $P = 0.1\text{ MPa}$. To calculate the formation energy, we used H_2O , N_2 , CH_4 , and H_2 as standard electronic energies. Green, orange, red, and violet balls represent the Ir, Ru, O, and N, respectively.

4) $\text{NO} + \text{N} \rightarrow \text{N}_2\text{O}$

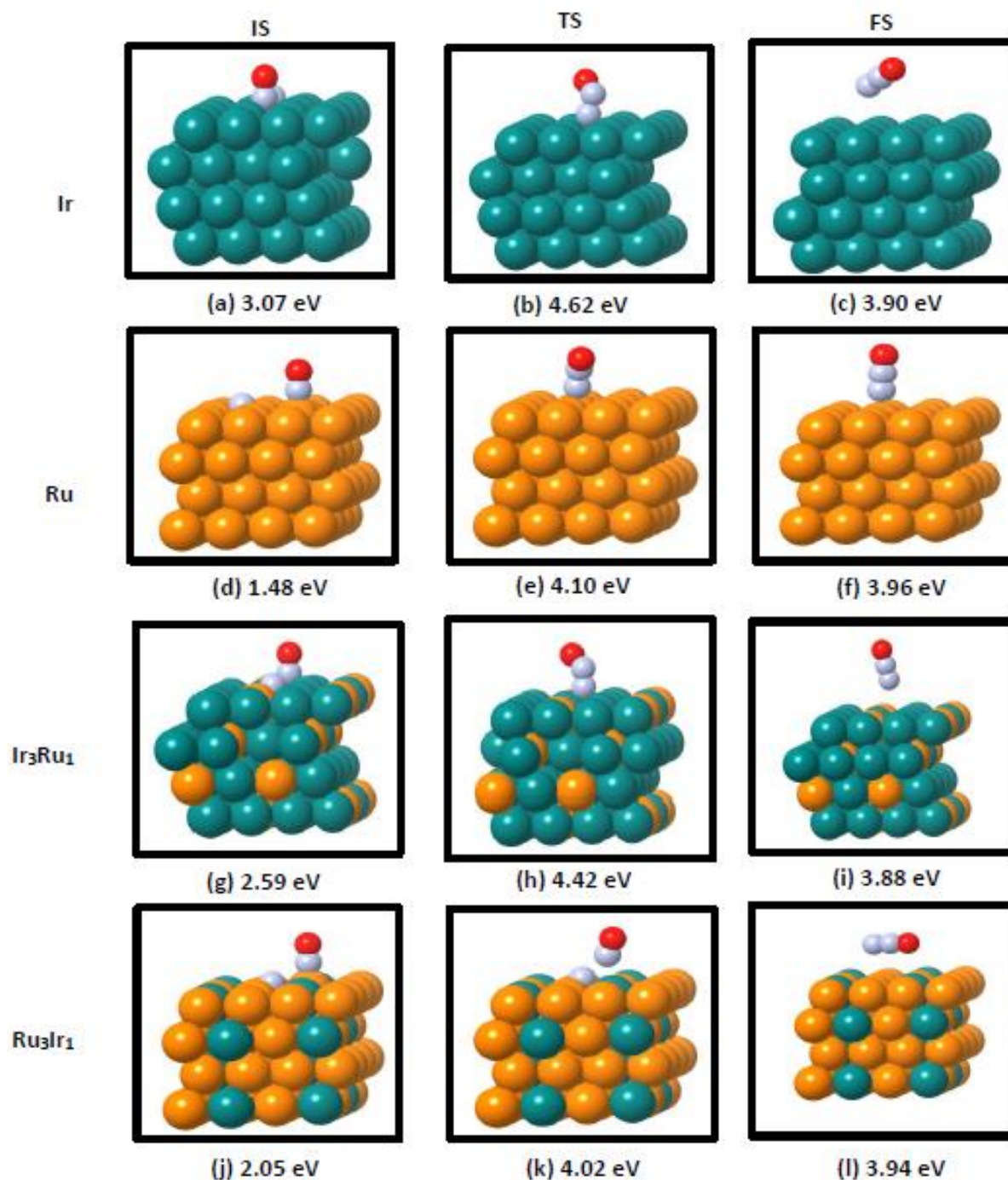


Fig. S27. Optimized geometry and gibbs free formation energy of N_2O formation reaction over Ir, Ru and their alloy surfaces at $T = 200\text{ }^\circ\text{C}$ and $P = 0.1\text{ MPa}$. To calculate the formation energy, we used H_2O , N_2 , CH_4 , and H_2 as standard electronic energies. Green, orange, red, and violet balls represent the Ir, Ru, O, and N, respectively.

5) $\text{N} + \text{CO} \rightarrow \text{NCO}$

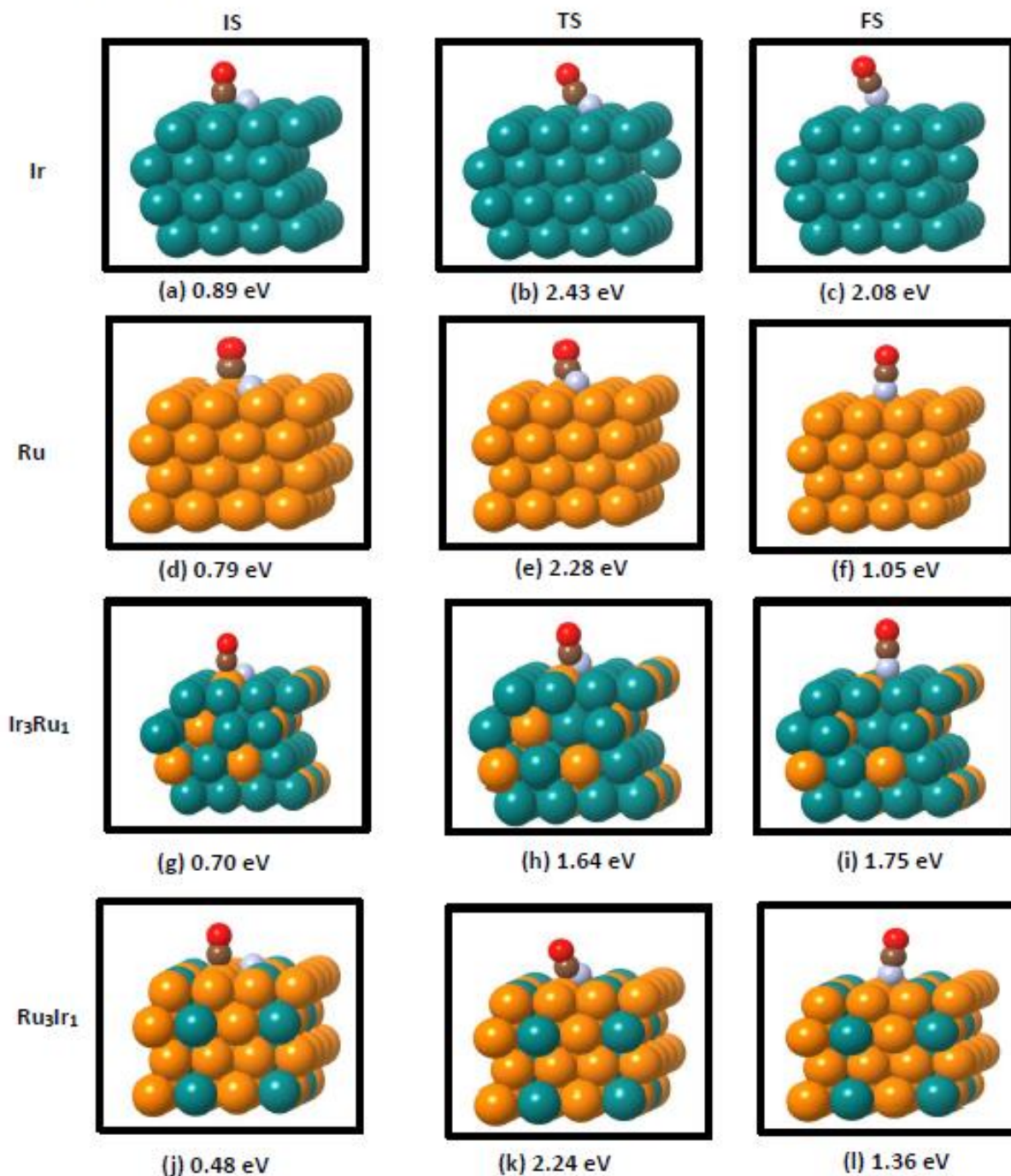


Fig. S28. Optimized geometry and gibbs free formation energy of NCO formation reaction over Ir, Ru and their alloy surfaces at $T = 200\text{ }^\circ\text{C}$ and $P = 0.1\text{ MPa}$. To calculate the formation energy, we used H_2O , N_2 , CH_4 , and H_2 as standard electronic energies. Green, orange, red, brown, and violet balls represent the Ir, Ru, O, C, and N, respectively.

6) $\text{NO} \rightarrow \text{N} + \text{O}$

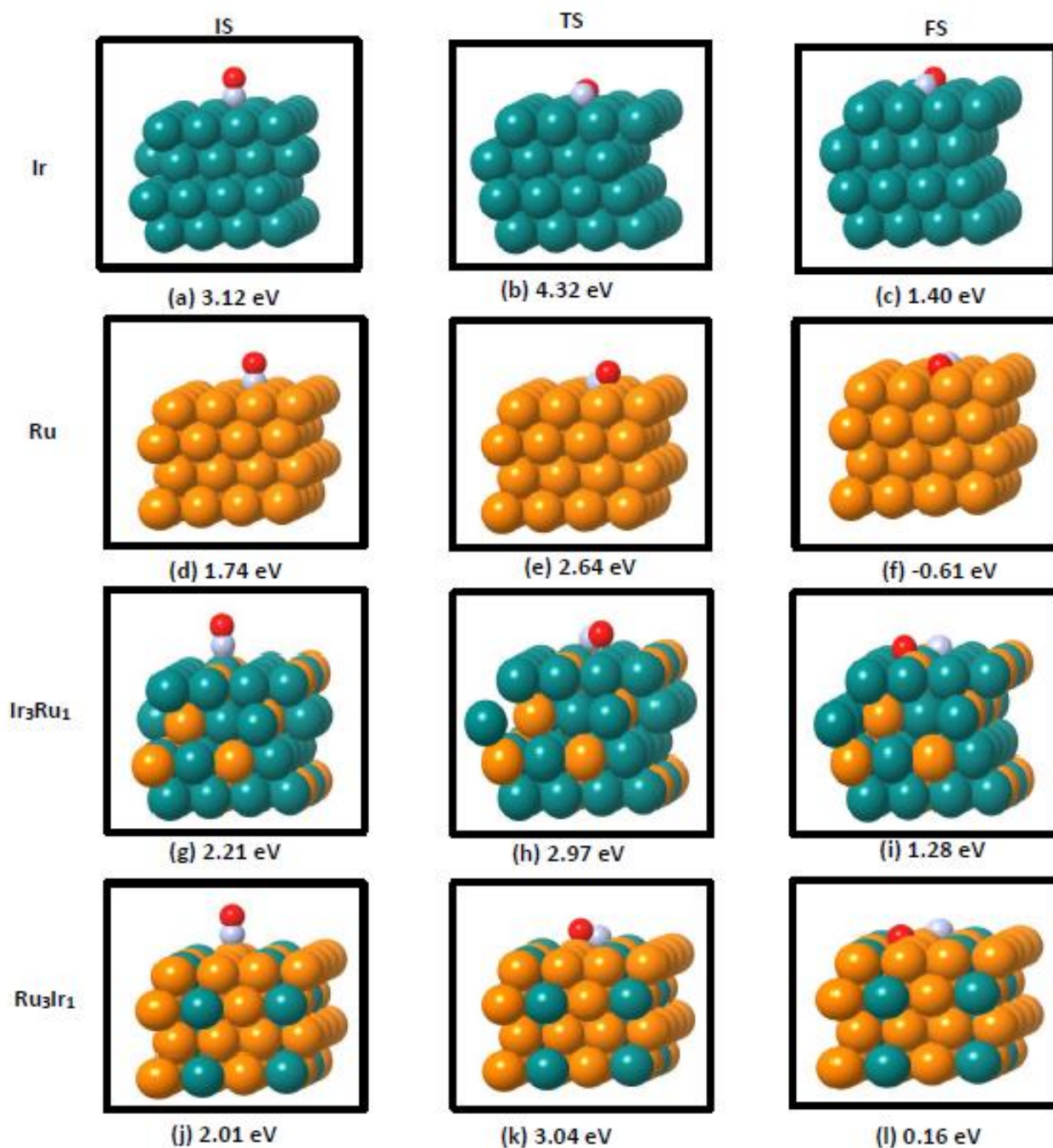


Fig. S29. Optimized geometry and gibbs free formation energy of NO decomposition reaction over Ir, Ru and their alloy surfaces at $T = 200 \text{ }^\circ\text{C}$ and $P = 0.1 \text{ MPa}$. To calculate the formation energy, we used H_2O , N_2 , CH_4 , and H_2 as standard electronic energies. Green, orange, red, and violet balls represent the Ir, Ru, O, and N, respectively.

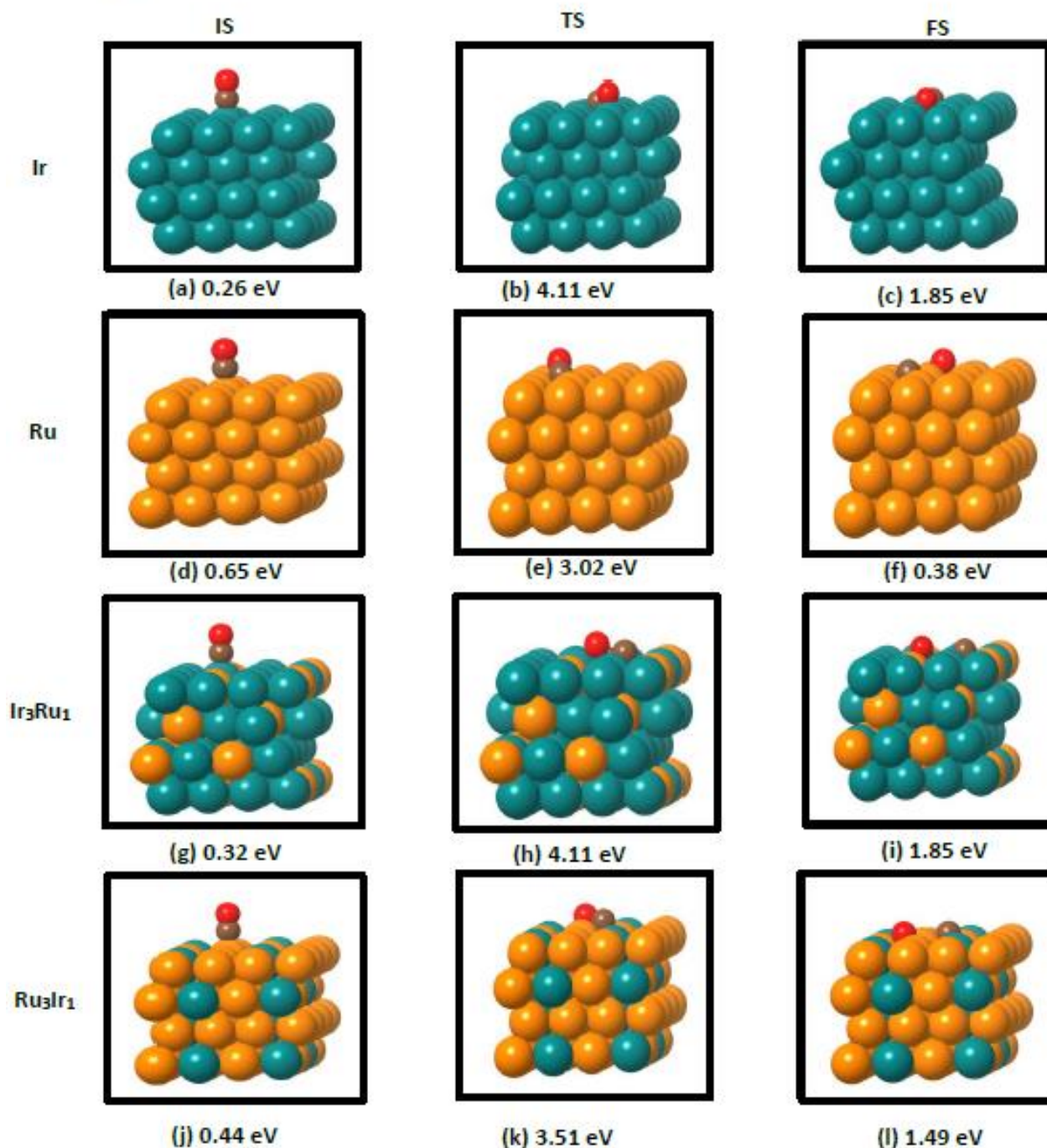


Fig. S30. Optimized geometry and gibbs free formation energy of CO decomposition reaction over Ir, Ru and their alloy surfaces at $T = 200\text{ }^\circ\text{C}$ and $P = 0.1\text{ MPa}$. To calculate the formation energy, we used H_2O , N_2 , CH_4 , and H_2 as standard electronic energies. Green, orange, red, and brown balls represent the Ir, Ru, O, and C, respectively.

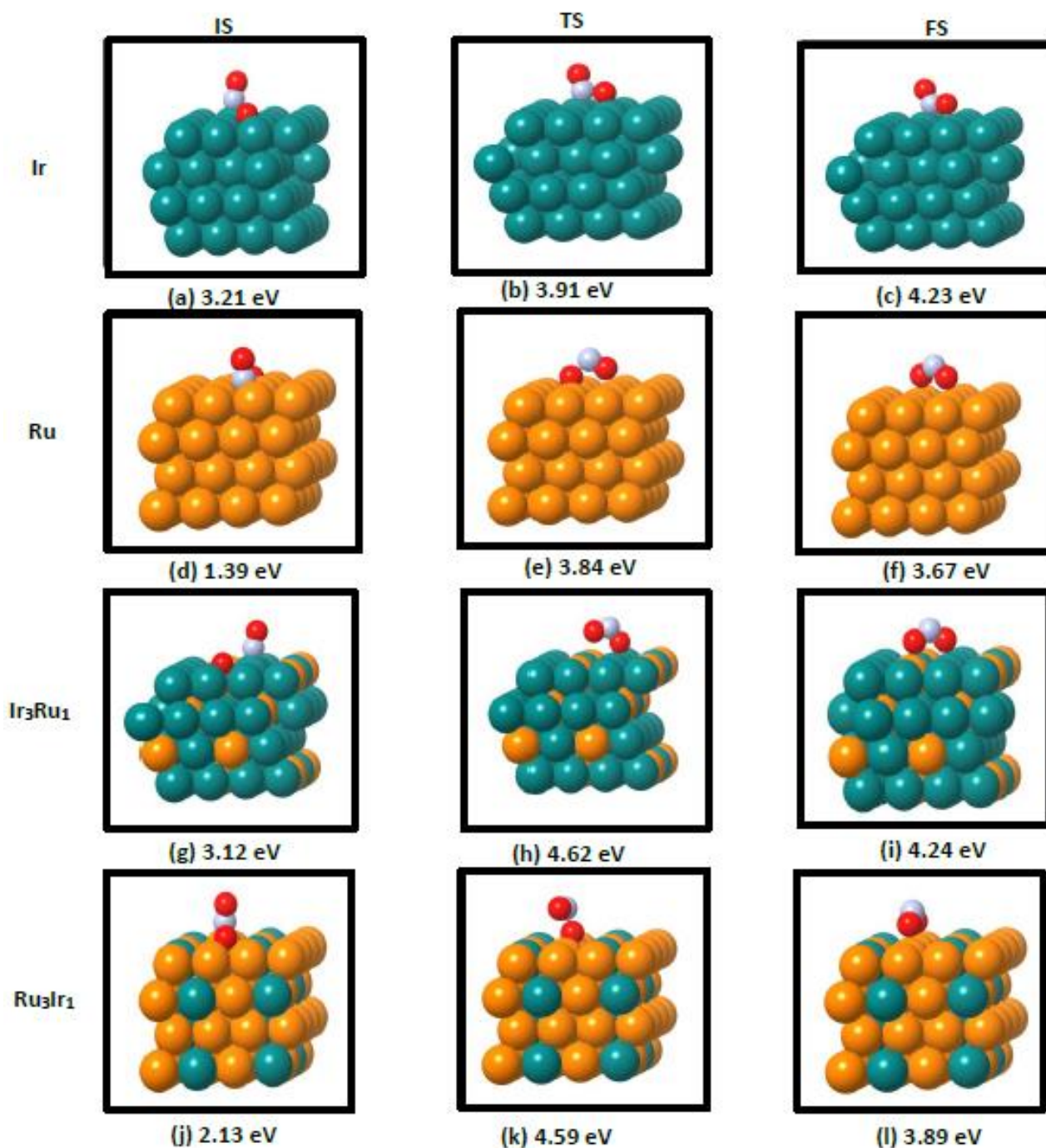
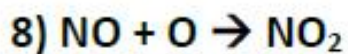


Fig. S31. Optimized geometry and gibbs free formation energy of NO_2 formation reaction over Ir, Ru and their alloy surfaces at $T = 200\text{ }^\circ\text{C}$ and $P = 0.1\text{ MPa}$. To calculate the formation energy, we used H_2O , N_2 , CH_4 , and H_2 as standard electronic energies. Green, orange, red, and violet balls represent the Ir, Ru, O, and N, respectively.

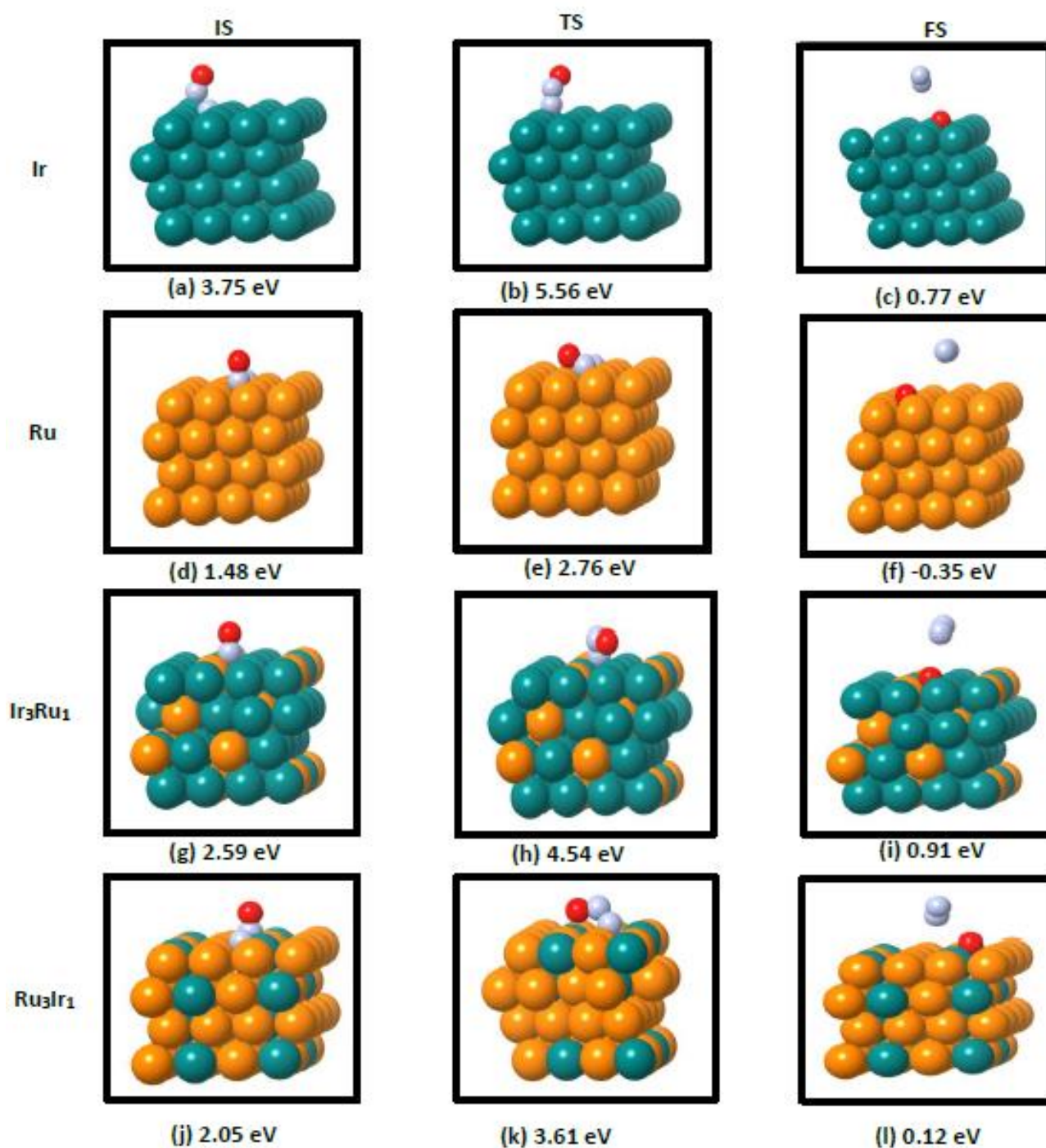
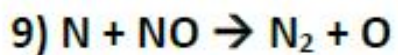


Fig. S32. Optimized geometry and gibbs free formation energy of N_2 formation reaction over Ir, Ru and their alloy surfaces at $T = 200\text{ }^\circ\text{C}$ and $P = 0.1\text{ MPa}$. To calculate the formation energy, we used H_2O , N_2 , CH_4 , and H_2 as standard electronic energies. Green, orange, red, and violet balls represent the Ir, Ru, O, and N, respectively.